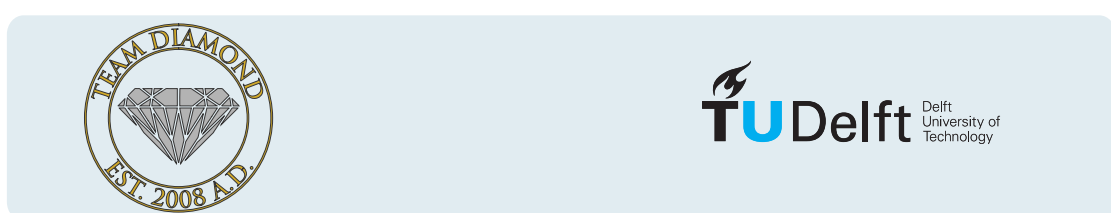


# Entanglement of Weakly-coupled Carbon-spins in Diamond

## MASTER OF SCIENCE THESIS

BY

Michiel Adriaan Rol



*Supervisors:*  
Ir.J.CRAMER,  
Dr. Ir. T.H.TAMINIAU,  
Prof. Dr. Ir. B HANSON

*Performed at:*  
Quantum Transport group  
Kavli Institute of Nanoscience  
Faculty of Applied Sciences, TU Delft



## **Abstract**

Quantum Error Correction is an essential ingredient for scaling up a quantum computer. The Nitrogen-Vacancy (NV) center in diamond is a promising candidate for such a scalable quantum computer. This thesis will first explain the basic tools available to control the NV-center in diamond and strongly coupled spins in the environment. We will then demonstrate how the spin register can be extended by addressing weakly coupled carbon-spins. The main result of this thesis is the creation of entanglement of these weakly coupled spins, for which initialization, control and read-out is required. We demonstrate entanglement with a fidelity of  $F = 0.76 \pm 0.02$ , well above the quantum limit for an entangled state. The last chapter will provide an outlook on how the capabilities developed can be used to implement QEC.



# Contents

<b>1</b>	<b>Introduction</b>	<b>5</b>
1.1	Quantum Computing . . . . .	5
1.2	Quantum Error Correction . . . . .	5
1.3	Weakly coupled carbons; a naturally occurring register . . . . .	5
<b>2</b>	<b>The Nitrogen-Vacancy center in Diamond</b>	<b>7</b>
2.1	The electronic spin . . . . .	7
2.1.1	Initialization and readout of the electronic-spin state . . . . .	8
2.1.2	Controlling the electronic-spin state . . . . .	8
2.2	Controlling nuclear spins . . . . .	8
2.2.1	The Hyperfine Interaction . . . . .	8
2.2.2	Controlling the nitrogen nuclear spin . . . . .	9
2.3	Decoherence . . . . .	9
2.3.1	Definition of strongly coupled . . . . .	10
<b>3</b>	<b>Addressing Weakly-coupled Carbon Spins</b>	<b>13</b>
3.1	Extending Electron Coherence . . . . .	13
3.1.1	Spin-Echo . . . . .	13
3.1.2	Dynamical Decoupling . . . . .	14
3.1.3	Dynamical decoupling spectroscopy . . . . .	14
3.2	Identifying weakly-coupled carbon-pins . . . . .	14
3.2.1	The effect of dynamical decoupling . . . . .	14
3.2.2	Response of a carbon-spin to dynamical decoupling spectroscopy . . . . .	16
3.2.3	Identifying Individual Carbon-spins . . . . .	16
3.2.4	Effect of the magnetic field . . . . .	17
3.3	Characterizing weakly-coupled carbon spins . . . . .	17
3.3.1	Basic operations . . . . .	17
3.3.2	Carbon Ramsey experiment . . . . .	18
<b>4</b>	<b>Controlling Weakly-coupled Carbon Spins</b>	<b>21</b>
4.1	Initialization and readout . . . . .	21
4.2	Parity measurement . . . . .	22
4.3	Demonstrating entanglement . . . . .	22
4.3.1	Tomography . . . . .	22
4.3.2	Result . . . . .	22
<b>5</b>	<b>Outlook: towards Quantum Error Correction</b>	<b>25</b>
5.1	Direct outlook, deterministic operations/what needs to be done/can be done . . . . .	25
5.2	Simulations, how many carbon can we control? . . . . .	25
<b>A</b>	<b>Fingerprintdata</b>	<b>29</b>

<b>B State Initialization</b>	<b>31</b>
B.1 Gates used	31
B.2 Initialization of the carbon-spin	31
<b>C Bell State Tomography</b>	<b>33</b>
<b>D Entanglement witness</b>	<b>35</b>
<b>E Simulations and Calculations for Number of Addressable Carbons</b>	<b>37</b>
E.1 Scaling of number of resonances with magnetic field	37
<b>F Constants and Experimental values</b>	<b>39</b>

# 1

## Introduction

An essential feature for a scalable quantum computer is the ability to correct for quantum errors. The Nitrogen-Vacancy center in diamond is a promising candidate for a scalable quantum computer. In order to perform

This chapter will explain why building a quantum computer is cool/important/essential/someotherbigword Explain why quantum error correction is essential in achieving this goal Requirements to perform quantum error correction Explain NV natural candidate Requirements 3-5 qubits + entanglement. This thesis will demonstrate how to address weakly coupled carbon spins and create entanglement between them.

### 1.1 Quantum Computing

The idea of using a quantum mechanical system to simulate physics was first explored by Feynman[6]. Because the Hilbert space(/state space?) of a quantum mechanical system scales exponentially with it's size one would need an exponentially large classical computer to simulate it's behavior. By manipulating a quantum mechanical system directly this scaling problem can be circumvented.

It was quantum simulation that eventually led to the idea of exploiting quantum effects to perform more efficient calculations but it wasn't until Shor's discovery of a remarkably efficient quantum algorithm for prime factorization in 1994[13] that quantum information science really took off.

Shor's algorithm was the first example where a quantum computer can provide an exponential speedup over a classical computer. Shor's and other quantum algorithms allow solving classes of problems that were previously unsolvable, a well known example being the breaking of classical encryption codes.

By now Shor's algorithm has been shown to work on a range of different small scale quantum computers [19] [Needs reference to Shor in different systems or basic algorithms in range of systems] but making a scalable quantum computer that can take full advantage of the exponential speedup proves elusive.

### 1.2 Quantum Error Correction

### 1.3 Weakly coupled carbons; a naturally occurring register

The Nitrogen Vacancy centre in diamond is a well investigated system[5] and a promising candidate for quantum computation[2]. In order to implement three qubit measurement based QEC we need three qubits plus ancillae that we can initialise, measure and conditionally perform operations on. These extra qubits are found in Carbon-13 atoms, which are normally a source of decoherence. These atoms can be addressed using a resonant decoupling sequence[15].



# 2

## The Nitrogen-Vacancy center in Diamond

The Nitrogen-Vacancy (NV) center in diamond provides a natural occurring qubit register in a solid state environment. This chapter will explain how the electronic-spin can be initialized, controlled and read-out and how the control over the electronic spin can be used to control nuclear spins. The control of nuclear spins is however limited by decoherence.

### 2.1 The electronic spin

The NV-center is a naturally occurring impurity in diamond consisting of a substitutional nitrogen and an adjacent lattice vacancy (Fig. 2.1a). The NV-center can be in a neutral charge state ( $\text{NV}^0$ ) and a negatively charged state ( $\text{NV}^-$ ). In this thesis we are mainly interested in the negatively charged state, where an additional electron is captured from the environment. In the  $\text{NV}^-$  state a spin-triplet is formed in the band gap by two electrons. This forms the basis of our qubit.

The electronic ground state can be described by the Hamiltonian [1]:

$$H_{\text{GS}} = \Delta S_z^2 + \gamma_e \mathbf{B} \cdot \mathbf{S} \quad (2.1)$$

Where  $S_i$  are the pauli-spin operators,  $\gamma_e = 2.802 \text{ MHz/G}$  the gyro-magnetic ratio and  $\Delta \approx 2.88 \text{ GHz}$  the zero-field splitting. In this expression the interactions with the nitrogen nucleus and the carbon spin bath are not included. In the experiments a magnetic field  $B_z = 304 \text{ G}$  is applied along the NV-axis<sup>1</sup>. The magnetic field lifts the degeneracy of the  $m_s = \pm 1$  states through the Zeeman effect.

We define our electronic qubit as the two level system  $m_s = 0 := |0\rangle$  and  $m_s = +1 := |1\rangle$ .

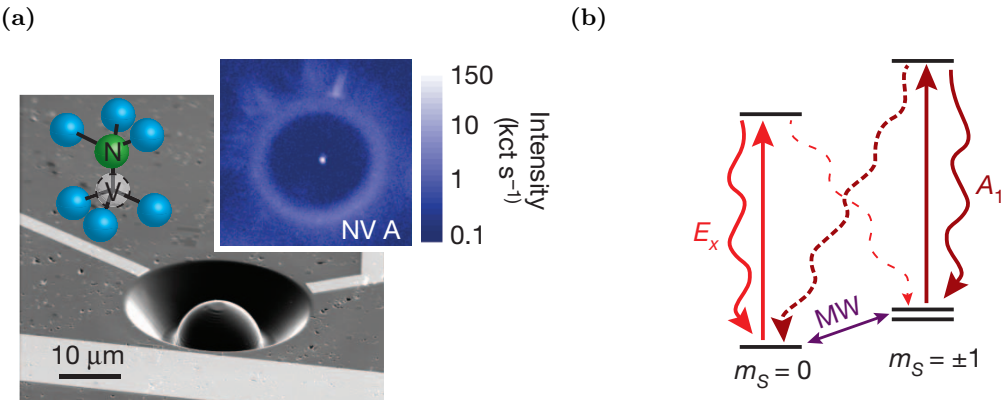


**Figure 2.1** – Figure 2.1a, Scanning electron microscope image of a solid immersion lens (SIL) similar to those used in the experiments. Overlaid sketch shows a schematic representation of the NV-center. Inset shows a scanning confocal microscope of an NV-center similar to those used in the experiments. Figure from [12]. Figure 2.1b, Energy levels used for initialization and readout of the electronic-spin state. Figure from [12]

<sup>1</sup>The NV-axis is the axis going through both the nitrogen and the vacancy.

### 2.1.1 Initialization and readout of the electronic-spin state

The transitions between the electronic ground-state and excited state are spin dependent and lie in the optical domain (637nm). At low temperatures these transitions can be resonantly excited using a laser of the corresponding frequency. The frequencies of these transitions depend on magnetic field and strain [9].

Figure 2.1b shows the optical transitions used to initialize and read-out the electronic spin. The  $A_1$  transition excites both the  $m_s = +1$  and the  $m_s = -1$  states to the excited state. The  $E_x$  transition excites the  $m_s = 0$  state to the excited state. When the spin falls back to the ground state there is a small probability that the spin is flipped, denoted by the dashed line.

Optically pumping one off these transitions will cause the spin-population to end up in the state that is not addressed and can be used to initialize the spin-state [12].

The optical transitions can also be used to read-out the spin state. By applying a pulse to the  $E_x$  transition a photon can be detected when the state falls back to the ground state. Because the  $E_x$  only excites the  $m_s = 0$  state photons can only be detected when the system is in the  $|0\rangle$ -state. By keeping the pulse short the probability that the spin flips is kept low.

Because the number of pumping cycles before the spin flips is limited the fidelity is limited by how well the few photons that are emitted are detected. A solid immersion lens (SIL), visible in Fig. 2.1a, is milled onto the sample to maximize the detection efficiency.

Using these methods the experiments were performed at a readout fidelity  $F = 90.55 \pm 0.40\%$ .

### 2.1.2 Controlling the electronic-spin state

The state of a qubit can be represented as a vector on the Bloch-sphere where the  $|0\rangle$ -state lies at the north pole and the  $|1\rangle$ -state at the south pole. On the Bloch-sphere the state vector rotates around the quantization-axis with a frequency depending on the energy splitting between the two states; the Larmor frequency. For the NV-electronic spin the Larmor frequency is given by Eq. (2.2) and the quantization axis lies in the z-direction (towards  $|0\rangle$ ).

$$\omega_L = \Delta + \gamma_e B_z \quad (2.2)$$

By applying an external field a term is added to the Hamiltonian, changing the quantization-axis and thereby its evolution. By applying microwaves with the right frequency this can be used to selectively drive the transition from the  $|0\rangle$  state to the  $|1\rangle$  state[10]. Resonant microwave pulses are applied to the sample trough on-chip lead, visible in Fig. 2.1a as the light area just below the SIL.

## 2.2 Controlling nuclear spins

The electronic-spin interacts with nuclear spins in its environment trough the hyperfine interaction. Close-by spins have a strong hyperfine interaction and can be controlled directly by applying microwave pulses. When the interaction is too weak the spins cannot be readily resolved and are a source of decoherence.

### 2.2.1 The Hyperfine Interaction

The coupling between the NV-centers electronic spin and a nuclear-spin is given by the hyperfine-interaction. The hyperfine-interaction is a spin dependent interaction that is not present for spin-0 particles such as carbon-12.

For nuclear spins the Hamiltonian depends on the electronic spin-state of the NV-center. For a magnetic field ( $B_z$ ) in the z-direction the Hamiltonian is given by Eq. (2.3) when the electronic-spin is in the  $m_s = 0$  state, and by Eq. (2.4) when in the  $m_s = +1$  state[17]. Where  $\mathbf{I}$  and  $\mathbf{S}$  are the nuclear and electronic spin operators,  $\gamma_n$  is the gyro-magnetic ratio of the nucleus and  $Q = 2\pi \cdot 4.946\text{MHz}$  is the nuclear quadrupole splitting of the nitrogen. The quadrupole term is not present when the nuclear spin is not a Nitrogen.

$$H_0 = -Q\mathbf{I}_z^2 + \gamma_n B_z I_z \quad (2.3)$$

$$H_1 = -Q\mathbf{I}_z^2 + \gamma_n B_z I_z + H_{HF} \quad (2.4)$$

The Larmor frequency for a nucleus is given by Eq. (2.5).

$$\omega_L = -Q\mathbf{I}_z^2 + \gamma_n B_z \cdot \hat{\mathbf{z}} \quad (2.5)$$

The hyperfine ( $H_{\text{HF}}$ ) term consists of a contact term and a dipole term. The contact term results from an overlap between the electronic- and nuclear- wave-functions. The contact term is negligible for all but the nuclear-spins closest to the NV-center. For close-by carbon spins hyperfine couplings have been calculated[7, 8] and measured measured[14].

For carbons where the contact term is negligible the hyperfine-term is equal to the dipole term and is given by Eq. (2.6)[3].  $\mathbf{n}_{\text{HF}}$  is a unit vector pointing from the electronic spin to the nucleus,  $r$  is the distance between the electronic and nuclear spin, and  $\mu_0$  the magnetic permeability.

$$H_{\text{dip}} = \frac{\mu_0 \gamma_e \gamma_C \hbar^2}{4\pi r^3} [\mathbf{S} \cdot \mathbf{I} - 3(\mathbf{S} \cdot \hat{\mathbf{n}}_{\text{HF}})(\mathbf{I} \cdot \hat{\mathbf{n}}_{\text{HF}})] \quad (2.6)$$

From Eq. (2.6) the parallel and orthogonal components of the Hyperfine interaction, with respect to the NV-axis along the z-direction, can be derived to be:

$$A_{\parallel} = -\frac{\mu_0 \gamma_e \gamma_C \hbar^2}{4\pi r^3} \left( 3 \cdot \frac{z^2}{r^2} - 1 \right) \quad (2.7)$$

$$A_{\perp} = -\frac{\mu_0 \gamma_e \gamma_C \hbar^2}{4\pi r^3} \left( 3 \cdot \frac{\sqrt{x^2 + y^2} \cdot z}{r^2} \right) \quad (2.8)$$

Where  $H_{\text{HF}} = A_{\parallel} I_z + A_{\perp} I_x$ .

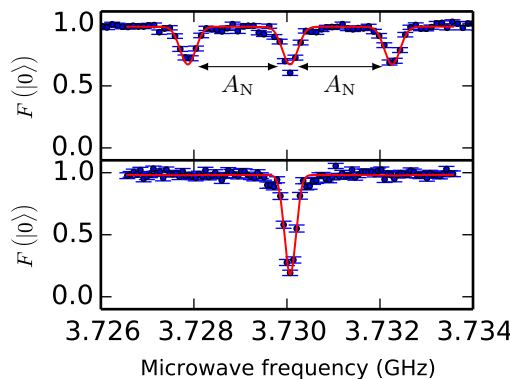


**Figure 2.2** – Electron Spin Resonance (ESR) for uninitialized (top) and initialized nitrogen spin (bottom) of the  $m_s = 0 \rightarrow m_s = +1$  transition. In a dark ESR the spin is prepared in  $|0\rangle$ , a microwave pulse is applied and then the  $|0\rangle$  state is read-out again. This is done for a range of frequencies. When the microwave is on resonance with a transition the spin will be rotated and a dip will be visible in the signal. In the top figure the transition is split due to the interaction with the nearby nitrogen atom. In the lower figure the nitrogen state is initialized and the splitting disappears.

### 2.2.2 Controlling the nitrogen nuclear spin

An example of a strongly coupled spin is the NV-nitrogen spin. The strength of the coupling between the nitrogen and the electronic spin is  $A_N = 2\pi \cdot 2.186 \text{ MHz}$ [1] and it acts along the NV-axis. Figure 2.2 clearly shows the  $m_s = 0 \rightarrow m_s = +1$  transitions being split due to hyperfine-coupling to the nitrogen. This splitting can be used to control the nitrogen. By first initializing in the  $m_s = +1$ -state and then applying a slow pulse that turns only one of the three nitrogen spin-states back to  $m_s = 0$  and reading out the nitrogen-spin can be initialized. By only continuing on a positive outcome the spin is initialized in the state that was rotated back to  $m_s = 0$ . We call this measurement-based-initialization (MBI). The lower panel of Fig. 2.2 shows a Electron-Spin-Resonance (ESR) after nitrogen-MBI.

In a similar way strongly-coupled carbon-13 atoms can be controlled[12].

## 2.3 Decoherence

When addressing a spin qubit we usually drive transitions between energy levels. When the electronic-spin couples to a nuclear-spin these energy levels are shifted depending on the state of the nucleus. In this way each spin has an individual back-action on the electronic-spin.

Most of these spins only shift the spin by a tiny amount making it hard to distinguish them from each other. Because the states of these spins fluctuate the transitions of the NV-center are continuously shifting around, effectively causing a broadening of the transitions. We call these very-weakly-coupled spins the spin-bath.

If the coupling between a spin and the NV-center is strong enough it is possible to resolve and address its transitions. Transitions between energy levels can be resolved if the difference between them is larger than the width of the transition.

How narrow a transition is related to how accurately it can be addressed. The largest variations in the spin-bath, that determine the position of the transition, occur between experiments.<sup>1</sup> Need to add some sentences here about why T2 star is measurement for this! The time before a transition shifts out of resonance, or a signal decoheres, is usually expressed by  $T_2^*$  and is measured by a Ramsey experiment, see Fig. 2.3a.

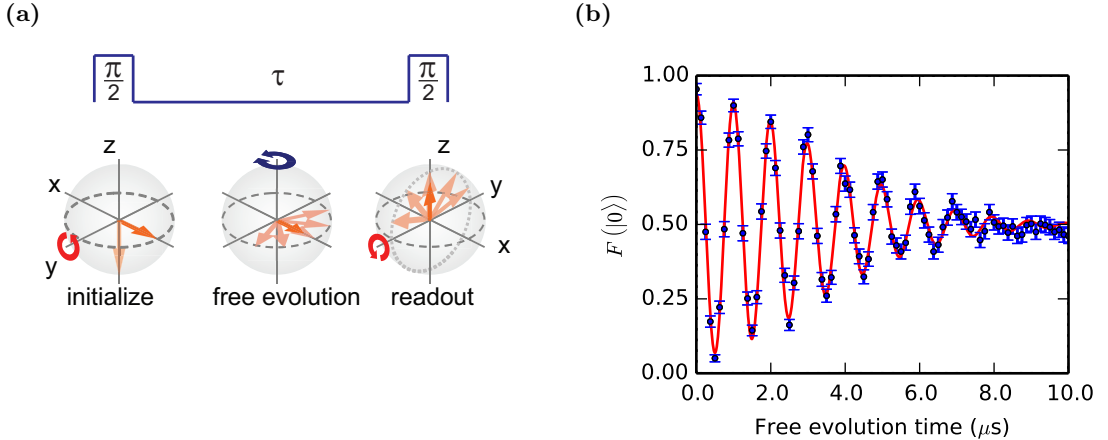


**Figure 2.3** – Figure 2.3a, schematic representation of a Ramsey experiment. Figure from de Lange [3]. In a Ramsey experiment a qubit is initialized along the z-axis before being subjected to a  $\pi/2$ -pulse that moves it into the XY-plane of the Bloch-sphere. It freely evolves for a time  $\tau$  before being subjected to a final  $\pi/2$  pulse and read out along the z-direction. By applying a detuning to the rotating frame the spin will pick up a phase  $\phi = \omega_d\tau$  during free evolution. The final pulse will rotate the spin towards the poles depending on the phase picked up during free evolution. This manifests itself as an oscillation. Because the configuration of the spin-bath is slightly different from experiment to experiment the frequency of the oscillation will vary from repetition to repetition. Figure 2.3b shows a Ramsey experiment for the electronic spin. A  $T_{2e}^*$  of  $4.54 \pm 0.14\mu\text{s}$  was measured for the electronic spin. The decay follows a Gaussian profile within uncertainty  $n = 1.81 \pm 0.14$ .

The decay of the amplitude  $K$  in an electron Ramsey experiment is given by Eq. (2.9).

$$K(\tau) = e^{-(\frac{\tau}{T_{2e}^*})^2} \quad (2.9)$$

We define  $T_{2e}^*$  as the  $1/e$  value of the Gaussian decay. The Electron-Spin-Resonance (ESR)<sup>2</sup> frequency spectrum for negligible power broadening is given by the Fourier transform of Eq. (2.9). Where  $\omega = 2\pi \cdot f^3$ .

$$\mathcal{F}\{K(\tau)\} = T_2^* \sqrt{\pi} e^{-\frac{(2\pi \cdot f)^2 \cdot T_{2e}^{*2}}{4}} \quad (2.10)$$

Two identical Gaussians can be readily resolved if the separation between their maxima is larger than their full-width-half-maximum (FWHM). The FWHM of the dark ESR is given by Eq. (2.11).

$$2\pi \cdot \text{FWHM} = 2\pi \cdot \frac{2\sqrt{\ln 2}}{\pi T_{2e}^*} \quad (2.11)$$

### 2.3.1 Definition of strongly coupled

We define a spin to be strongly coupled when it is possible to readily resolve its transition.

An estimation of when spins can be resolved can be made by looking at the strength of the hyperfine interaction. The splitting caused by a carbon spin is equal to twice the total interaction

<sup>2</sup>See Fig. 2.2 for an example of a dark ESR.

<sup>3</sup>For clarity the factor of  $2\pi$  is stated explicitly throughout this thesis to distinguish real and angular frequency.

strength  $A$  at low magnetic field ( $\gamma_e B \ll A$ ). In the limit of high magnetic field ( $\gamma_e B \gg A$ ) only the parallel component of the interaction  $A_{\parallel}$  contributes to the splitting. We can readily resolve a transition when the shift due to the corresponding interaction is larger than the FWHM of the transition.

$$2\pi \cdot |\mathbf{A}| \gg 2\pi \cdot \frac{\sqrt{\ln 2}}{\pi T_{2e}^*}, \quad \text{for } \gamma_e B \ll A \quad (2.12)$$

$$2\pi \cdot A_{\parallel} \gg 2\pi \cdot \frac{\sqrt{\ln 2}}{\pi T_{2e}^*}, \quad \text{for } \gamma_e B \gg A \quad (2.13)$$

NV-centers have a typical electron  $T_{2e}^* \approx 2\mu\text{s}$ <sup>4</sup> that depends on the exact configuration of the spin-environment. On the sample used for the experiments  $T_{2,e}^* = 4.54 \pm 14\mu\text{s}$  was measured, see Fig. 2.3b. Increasing the carbon-13 concentration generally reduces  $T_{2e}^*$ . For a typical NV-center this means that the coupling between the carbon and the NV-center must be larger than  $2\pi \cdot 130\text{kHz}$  for the carbon to be directly addressable for a typical NV-center and larger than  $2\pi \cdot 58\text{kHz}$  for our sample.

---

<sup>4</sup>At a natural concentration of 1.1% carbon-13.



# 3

## Addressing Weakly-coupled Carbon Spins

In order to be less dependent on the presence of strongly coupled nuclear spins weakly coupled spins can be addressed. This chapter will demonstrate how to extend electron coherence time so that weakly coupled spins can be resolved. Identify nuclear spins in the environment of our NV-center and characterize these spins.

The electronic-spin of the NV-center does not live in a vacuum but in an environment full of nuclear spins. To some of these spins the NV-center couples strongly, these spins can be controlled and can serve as qubits. To others it couples weakly these spins are a source of decoherence and cannot be controlled directly.

In this chapter I will first explain what strong and weakly coupled spins are, how this relates to coherence and how coherence can be extended through dynamical decoupling. In the second part of this chapter I will explain how dynamical decoupling can be used to identify and control some of these weakly coupled spins, transforming them from a source of decoherence to a resource for qubits.

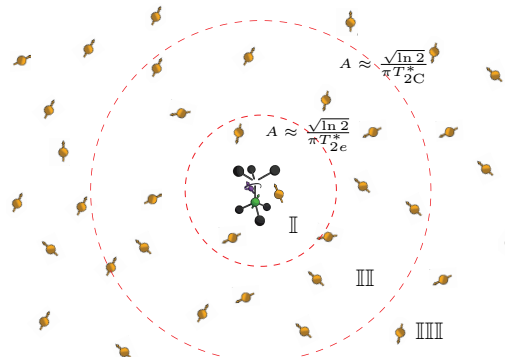


**Figure 3.1** – Schematic representation of different coupling regimes. In the strong coupling regime (region I) carbon-spins are coupled to the NV-center stronger than the coupling of the NV-center to the spin-bath. These carbons can be addressed directly. In the weak coupling regime (region III) carbon-spins are coupled more strongly to the NV-center than to the spin-bath but not strong enough to be addressed directly. In the very-weak coupling regime (region III) the coupling to the spin-bath is stronger than the coupling to the NV-center. These spins cannot be addressed.

### 3.1 Extending Electron Coherence

#### 3.1.1 Spin-Echo

In a spin-echo experiment a Ramsey experiment is performed with a small difference. An additional  $\pi$  pulse is applied in the middle of the experiment exactly between the  $\pi/2$  pulses. This pulse effectively turns the nuclear-spin environment upside-down halfway through the experiment, making the quasi-static-part of the dephasing during the first and the second part of the free evolution

cancel each other out, substantially increasing coherence on short-timescales ( $\tau \ll T_2$ )<sup>1</sup>. On longer timescales the difference between the initial part of the evolution and the final part of the evolution becomes larger making the initial and final part no longer cancel each other out.

### 3.1.2 Dynamical Decoupling

A natural way of extending the short timescale behavior of the spin-echo to longer timescales is by applying more  $\pi$ -pulses. This procedure known as dynamical-decoupling can dramatically improve coherence times by decoupling the central-spin from the environment[4].

Although dynamical-decoupling improves the coherence of the central spin by decoupling from the environment, the central spin is also decoupled from other spins preventing direct two-qubit gates. It was demonstrated by van der Sar et al. [18] how to incorporate dynamical decoupling in a universal gate design by implementing Grover's algorithm. Using this technique Taminiau et al. [16] used the extended coherence to detect and control weakly-coupled carbon spins, before implementing three-qubit quantum-error-correction (QEC) [17].

As these experiments were performed with NV-centers at Room temperature they lack the option to do single-shot readout required to act on a measurement outcome<sup>2</sup>. An essential feature for the parity measurements that form the basis of measurement-based QEC and surface codes.

### 3.1.3 Dynamical decoupling spectroscopy

As we cannot perform an ESR experiment while decoupling a different technique must be used to resolve and address additional spins. In order to resolve additional spins we perform a dynamical decoupling spectroscopy, resulting in a fingerprint of the nuclear-spin environment[16].

In a dynamical decoupling spectroscopy experiment the electron is prepared in the  $|X\rangle = |0\rangle + |1\rangle$  state. It is subjected to a decoupling sequence consisting of  $N/2$  blocks of the form  $\tau - \pi - 2\tau - \pi - \tau$ , and concluded by measuring  $\langle X \rangle$ . The fingerprint is the result of many repetitions for a range of inter-pulse delays  $2\tau$ .  $\pi$  is a  $\pi$ -pulse.

Part of a dynamical decoupling spectroscopy can be seen in Fig. 3.2. The spectroscopy was performed for  $N = 8, 16, 32$  and  $64$  pulses. For  $N = 8, 16$  and  $32$  pulses this was done between  $\tau = 2\mu s$  and  $72\mu s$  and for  $N = 64$  this was done up to  $\tau = 52\mu s$ . A reference to the full spectroscopy can be found in Appendix A.

## 3.2 Identifying weakly-coupled carbon-pins

In order to understand how the features in the fingerprint from Fig. 3.2 relate to the different spins and how this knowledge can be used to control these carbons it is necessary to understand what dynamical decoupling does to these atoms.

### 3.2.1 The effect of dynamical decoupling

When the electron is in the  $m_s = 0$  state each nuclear spin precesses about  $\omega_L$  with the Larmor frequency. When the electron is in the  $m_s = +1$  state nuclear spins precess about a distinct axis  $\tilde{\omega} = \omega_L + \mathbf{A}$  [16]. The hyperfine interaction  $\mathbf{A}$  depends on the position of that particular nuclear spin relative to the NV- center.

When applying a decoupling sequence with  $N/2$  decoupling units of the form  $\tau - \pi - 2\tau - \pi - \tau$ , the nuclear spin alternately rotates around the  $\omega_L$  and the  $\tilde{\omega}$  axis. The net result of one such decoupling sequence is a rotation around an axis  $\hat{\mathbf{n}}_i$  by an angle  $\phi$ . Where  $\hat{\mathbf{n}}_i$  depends on the initial state of the electron:  $\hat{\mathbf{n}}_0$  when the electron starts in  $m_s = 0$  and  $\hat{\mathbf{n}}_1$  when the electron starts in  $m_s = +1$  [16].

To understand how a carbon-13 atom can be controlled it is useful to consider three situations. In the first situation the  $\omega_L$  and  $\mathbf{A}$  point in the same direction. In the second situation  $\omega_L$  and  $\mathbf{A}_\perp$  are of comparable magnitude, resulting in a large angle between the quantization axes. In the last situation  $|\mathbf{A}|$  is small compared to  $|\omega_L|$  resulting in a small angle between the quantization axes.

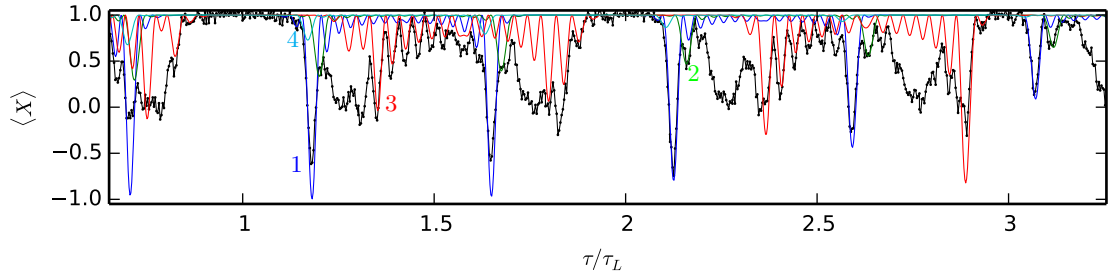
When  $\omega_L$  and  $\mathbf{A}$  point in the same direction, the net rotation axis is independent of the initial electron-state making it impossible to use the electron to control the carbon-13 atom using this decoupling sequence.

---

<sup>1</sup>  $T_2$  is a measure for decoherence. It is similar to  $T_2^*$  but does not include variations between experiments.  $T_2$  is defined as the  $1/e$  time of the decay of a spin-echo experiment.

<sup>2</sup>@Tim, I think this can be worded more concisely. Do you have any ideas?

(a)



(b)

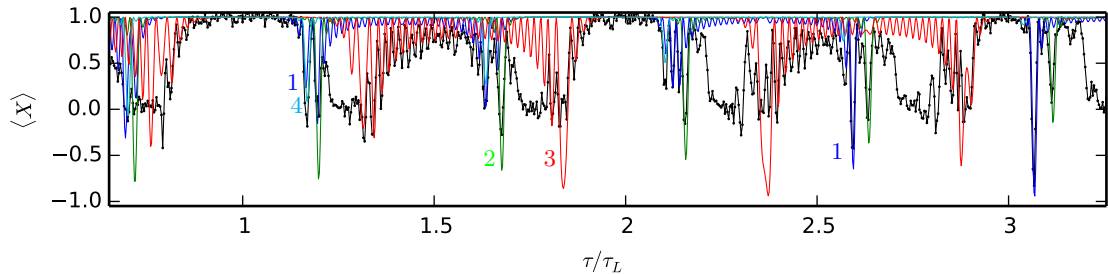


**Figure 3.2** – Part of a fingerprint resulting from a dynamical-decoupling-spectroscopy experiment performed at 304G. A reference to the full spectroscopy can be found in Appendix A. Colored lines represent computed responses of carbon spins. Responses were calculated using Eq. (3.4) with hyperfine parameters from Table 3.1.

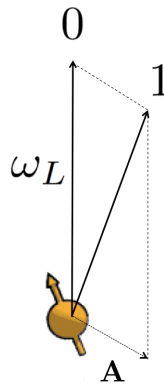
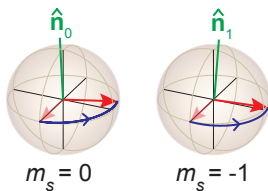


**Figure 3.3** – Flipping the electron spin from the  $m_s = 0$  to the  $m_s = +1$  state changes the quantization axis of nuclear spins. For  $m_s = 0$  all nuclear spins precess about  $\omega_L$ . For  $m_s = +1$  each spin precesses about a distinct axis  $\tilde{\omega} = \omega_L + \mathbf{A}$ .

(a)



(b)

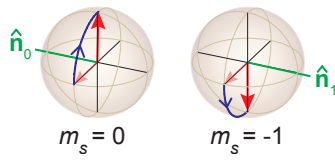


**Figure 3.4** – Figure 3.4a When the net rotation axes  $\hat{n}_0$  and  $\hat{n}_1$  point in the same direction the carbon experiences an unconditional rotation and cannot be controlled. Figure 3.4b When the net rotation axes  $\hat{n}_0$  and  $\hat{n}_1$  are anti-parallel the carbon experiences a conditional rotation, either around  $+x$  or  $-x$ , and can be controlled.

In the case where  $\omega_L$  and  $A_{\perp}$  are of comparable magnitude the net rotation axes  $\hat{\mathbf{n}}_i$  are strongly dependent on the initial electron-state for almost any  $\tau$ . This creates entanglement between the electron and this carbon for a wide range of inter pulse-delays  $\tau$ . For future reference we say that these weakly-coupled carbons are in the *complex regime*.

When considering the case where the hyperfine interaction is much smaller than the Larmor frequency ( $\omega_L \gg |A|$ ), the net rotation axes  $\hat{\mathbf{n}}_0$  and  $\hat{\mathbf{n}}_1$  are practically parallel and the nuclear spin undergoes an unconditional evolution. Only when the inter-pulse delay is precisely resonant with the spin dynamics the axes are anti-parallel leading to a conditional rotation[16]. The resonant condition is given by Eq. (3.1), where  $k$  is an integer and the FWHM of the Lorentzian-shaped resonance is given by Eq. (3.2). To distinguish these carbons from those in the complex regime we say that these weakly-coupled carbons are in the *basic regime*.

$$\tau = \frac{(2k+1)\pi}{2\omega_L + A_{\parallel}} \quad (3.1)$$

$$\Delta = \frac{A_{\perp}}{2\omega_L^2} \quad (3.2)$$

If  $\hat{\mathbf{n}}_0$  and  $\hat{\mathbf{n}}_1$  are not parallel, the resulting conditional rotation of the nuclear spin generally entangles the electron and nuclear spins.

### 3.2.2 Response of a carbon-spin to dynamical decoupling spectroscopy

As a result the electronic spin, starting out in  $|X\rangle$ , entangles with the nuclear spin for specific values of  $\tau$  during a dynamical decoupling spectroscopy. When reading out the electronic spin along the X-axis this creates a dip in the signal. The probability that the initial state is preserved is given by Eq. (3.3). Where the contrast  $M_j$  for a single nuclear spin is given by Eq. (3.4)[16].

$$P_x = (M + 1)/2 \quad (3.3)$$

$$M_j = 1 - (1 - \hat{\mathbf{n}}_0 \cdot \hat{\mathbf{n}}_1) \sin^2 \frac{N\phi}{2} \quad (3.4)$$

$$1 - \hat{\mathbf{n}}_0 \cdot \hat{\mathbf{n}}_1 = \frac{A_{\perp}^2}{\tilde{\omega}^2} \frac{(1 - \cos(\tilde{\omega}\tau))(1 - \cos(\omega_L\tau))}{1 + \cos(\tilde{\omega}\tau) \cos(\omega_L\tau) - (\frac{A_{\parallel} + \omega_L}{\tilde{\omega}}) \sin(\tilde{\omega}\tau) \sin(\omega_L\tau)} \quad (3.5)$$

$$\phi = \cos^{-1} \left( \cos(\tilde{\omega}\tau) \cos(\omega_L\tau) - \left( \frac{A_{\parallel} + \omega_L}{\tilde{\omega}} \right) \sin(\tilde{\omega}\tau) \sin(\omega_L\tau) \right) \quad (3.6)$$

In reality the electron is not interacting with a single carbon but with a bath of carbon atoms. When the electron interacts with multiple carbons at the same time the contrast  $M$  is given by the product of all individual values  $M_j$  for each individual spin  $j$  (Eq. (3.7)). In order to selectively control one carbon the electron should not entangle with any other carbon when addressing it.

$$M = \prod_j M_j \quad (3.7)$$

When entanglement is created with multiple carbons at the same time coherence is quickly lost and contrast drops to 0. By sweeping the number of pulses  $\pi$ -pulses the response of an individual carbon can be distinguished from the response of multiple spins. Only when an individual carbon is being addressed is it possible to sweep the contrast to -1.

### 3.2.3 Identifying Individual Carbon-spins

By identifying distinct dips in the fingerprint, of which Fig. 3.2 shows a small part, we are able to make a first estimate of the hyperfine coupling using their location(Eq. (3.1)) and their width (Eq. (3.2)). We then compute the responses for these estimated hyperfine parameters using Eq. (3.4). The parameters are varied until the computed response agrees with the data as well as possible to arrive at a more accurate estimation of the hyperfine parameters. Using this method 13 distinct carbon spins were identified.

The parameters of the 4 strongest coupled carbons are listed in Table 3.1 and their computed responses are visible as colored lines in Fig. 3.2. All estimated hyperfine parameters and a link to the full fingerprint measurements can be found in Appendix A.

Carbon	$A_{\parallel}$	$A_{\perp}$
1	$2\pi \cdot 30.0$ kHz	$2\pi \cdot 80.0$ kHz
2	$2\pi \cdot 27.0$ kHz	$2\pi \cdot 28.5$ kHz
3	$2\pi \cdot 51.0$ kHz	$2\pi \cdot 105.0$ kHz
4	$2\pi \cdot 45.1$ kHz	$2\pi \cdot 20.0$ kHz

**Table 3.1** – Estimated hyperfine parameters for spins 1 to 4 in Fig. 3.2.

Most spins are relatively far away from the NV-center and have similar hyperfine couplings causing their resonances to overlap. This causes a broad feature with low coherence known as the spin-bath collapse. This feature is clearly visible in the fingerprint (Fig. 3.2) at  $\tau/(4\tau_L) = m$  for odd  $m$ , where  $\tau_L$  is the Larmor period ( $\tau_L = \frac{2\pi}{\omega_L}$ ).

Spins that have a stronger than average hyperfine-interaction show up outside or at the edge of the spin-bath collapse. Spins that are in the basic regime show up as a narrow dip. Going to larger  $\tau$  separates these dips further as the order of the resonance  $k$  increases. By looking at larger  $\tau$  it is possible to resolve and address more resonances. Several spins in the basic regime have been identified 3 of these are visible as colored lines in Fig. 3.2. As computations are fundamentally limited by the coherence time there is a limit to the resonance-order that can be used to address carbons, making it impossible to resolve all weakly coupled spins.

Besides the carbons in the basic regime there are also weakly-coupled carbons that are more strongly coupled. When a carbon in the complex regime is present in the NV-center this manifests itself as a resonance with strong oscillations on the side. Such a feature is also clearly visible in Fig. 3.2. We have identified the oscillations in the fingerprint as belong to a single spin which is denoted by the red line.

When a weakly coupled carbon in the complex regime is present a significant part of the fingerprint spectrum is inaccessible for controlling other carbons making them an undesired feature when attempting to control weakly coupled carbon spins.

### 3.2.4 Effect of the magnetic field

There are significant advantages to increasing the magnetic field when attempting to address weakly coupled carbons. By increasing the magnetic field the Larmor frequency can be increased, reducing the number of carbons that are in the complex regime. This causes the broad oscillating resonances to disappear allowing more carbons to be addressed.

Although increasing the magnetic field can improve the situation it is not always possible or desired. When the magnetic field becomes too strong too strong the resonances become narrower than the resolution of the Arbitrary Waveform Generator used to generate the pulses that address the resonances, making it impossible to address these resonances effectively. Simulations were performed (see Appendix E) that indicate that for a natural carbon-13 concentration there is a range between 400G and 1400G where the magnetic field is optimal for controlling weakly coupled spins.

Besides the spin environment there are other factors affecting the choice for magnetic field. Because the optical transitions used for readout and initialization depend on strain and magnetic field field[9], care must be taken when measuring that states do not mix in the excited state. This combined with the fact that few experiments have been performed at high magnetic field and low temperature make it more practical to settle for a more moderate magnetic field of 300G.

## 3.3 Characterizing weakly-coupled carbon spins

This section will explain how a weakly-coupled spin can be controlled using the conditional rotation of the carbon spin that occurs when on resonance (Eq. (3.1)). It will start by explaining how to do basic gate operations in the ideal case of being perfectly on resonant and not interacting with any nuclear spins. After that we will explain how a carbon-spin in a mixed state can be initialized

### 3.3.1 Basic operations

As was explained in ?? nuclear spins perform a rotation along two anti-parallel axes when subjected to a dynamical decoupling sequence on a resonant condition given by Eq. (3.1). The angle of rotation can be controlled by choosing the number of pulses of the decoupling sequence.

By choosing the number of pulses such that all coherence is lost when performing a dynamical decoupling spectroscopy measurement on the resonance, a rotation of  $\pi/2$  in the clockwise direction is performed when the electron is in the  $|0\rangle$ -state and a  $\pi/2$ -rotation in the counterclockwise direction when the electron is in the  $|1\rangle$ -state. We define the axis of rotation of this operation as the X-axis.

We call this conditional rotation the  $\pm x$ -gate and it forms the basis of our control over weakly coupled spins. Figure 3.5 shows how we depict the  $\pm x$ -gate in a circuit-diagram. By letting the phase of the carbon evolve we are able to apply operations on the carbon-spin with arbitrary phase. An unconditional gate can be implemented by placing the electron in an eigenstate before performing the  $\pm x$ -operation.

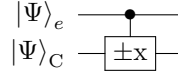


**Figure 3.5** – The conditional x-gate ( $\pm x$ ). Performs an x-rotation on the carbon state ( $|\Psi\rangle_C$ ) when the electron is in the  $|0\rangle_e$ -state. It performs a  $-x$  rotation when the electron is in the  $|1\rangle_e$ -state.

Basic gates can be calibrated by sweeping the number of pulses  $N$  when on resonance  $\tau$ . In this manner carbon-1 and carbon-4 were found to perform the best  $\pm x$ -gates. The parameters used to implement  $\pm x$ -gates are listed in Table 3.2.

Carbon	$N$	$\tau$	total gate time
1	18	9.420 $\mu s$	339 $\mu s$
2	26	6.620 $\mu s$	344 $\mu s$
3	14	18.564 $\mu s$	520 $\mu s$
4	40	6.456 $\mu s$	516 $\mu s$

**Table 3.2** – Parameters used to implement  $\pm x$ -gates.

### 3.3.2 Carbon Ramsey experiment

By performing a Ramsey experiment we can determine the precession of the carbon-spin and its dephasing-time  $T_2^*$ . By determining the precession frequencies it is possible to track phase evolution and use that to implement operations with arbitrary phase. By measuring the precession frequency it is also possible to disprove our estimation for the hyperfine parameters. We require the dephasing time in order to determine if enough operations can be applied to implement quantum algorithms<sup>3</sup>.

In an ordinary Ramsey experiment a qubit is brought to the equator of the Bloch-sphere where it precesses for a time  $\tau$  before it is read out along the x-direction. A carbon-Ramsey experiment is similar but slightly more complicated as the nuclear spin cannot be controlled and read-out directly. An uninitialized and an initialized version are depicted in Fig. 3.6.

In the initialized version of the carbon-Ramsey experiment the system is first initialized in the  $|0\rangle_e|X\rangle_C$ -state. The carbon is let to precess for a time  $\tau$  before the  $|X\rangle_C$ -state is read out. During the free evolution the carbon rotates with a frequency of  $\omega_L$  because the electron is in  $|0\rangle_e$  and there is no coupling.

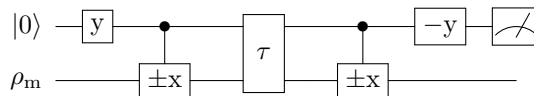


**Figure 3.6** – Gate circuit depicting a carbon Ramsey with

### Determining the precession frequency

A conceptually more interesting variety is the uninitialized carbon-Ramsey experiment depicted in ???. In the uninitialized version the system is described by Eq. (4.2) before the free evolution starts. Because the electron is in a superposition of  $|0\rangle$  and  $|1\rangle$  the carbon-spin while evolve with two frequencies;  $\omega_L$  for  $|0\rangle_e$  and  $\tilde{\omega} = |\omega_L + \mathbf{A}|$  for  $|1\rangle_e$ .

Similar to how the last part of the initialized carbon-Ramsey circuit reads out along the X-direction the last part of the uninitialized carbon-Ramsey reads out along the X-direction for the

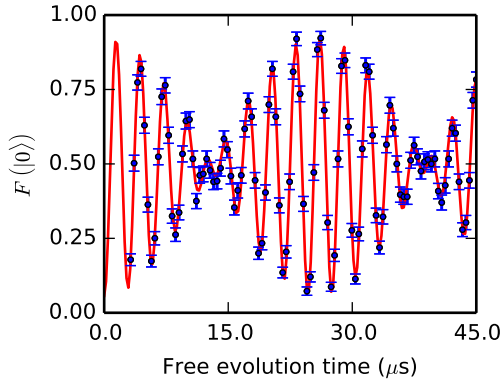
<sup>3</sup>Change this sentence

$|Y\rangle_e$  and along the  $-X$ -direction for the  $| -Y \rangle_e$ . The phase picked up while show up as an oscillation between the  $|0\rangle$  and  $|1\rangle$  in the readout. If the carbon has picked up no phase the the electron will point towards  $|1\rangle$  in the readout. Because the uninitialized carbon-Ramsey evolves with two frequencies we expect the measured oscillation to be the sum of two cosines as described by Eq. (3.8).

Where  $\tilde{\omega} = \sqrt{(\omega_L + A_{\parallel})^2 + A_{\perp}^2}$ .

$$\frac{1}{4} \cos(\omega_L \tau) + \frac{1}{4} \cos(\tilde{\omega} \tau) + \frac{1}{2} \quad (3.8)$$

(a)



(b)

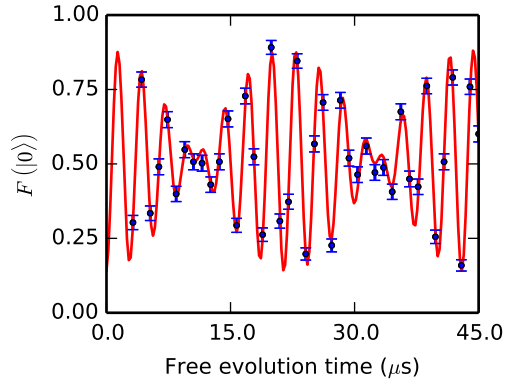


**Figure 3.7** – The uninitialized carbon-Ramsey experiment shows an oscillation that is the sum of two cosines due to the phase picked up during free evolution. Figure 3.7a depicts carbon-1 and Fig. 3.7b carbon-4. The measured frequencies were, for carbon-1:  $\omega_{L,C1} = 2\pi \cdot 325.81 \pm 0.25$  and  $\tilde{\omega}_{C1} = 2\pi \cdot 364.41 \pm 0.23$ , and for carbon-4:  $\omega_{L,C4} = 2\pi \cdot 325.94 \pm 0.40$  and  $\tilde{\omega}_{C4} = 2\pi \cdot 371.52 \pm 0.39$ .

Figure 3.7 shows the results for an uninitialized carbon-Ramsey experiment. The data was fitted to a sum of two cosines in order to determine the frequencies. The Larmor frequencies are  $\omega_{L,C1} = 2\pi \cdot 325.81 \pm 0.25\text{kHz}$  for carbon-1 and  $\omega_{L,C4} = 2\pi \cdot 325.94 \pm 0.40\text{kHz}$  for carbon-4. Both the measured Larmor frequencies agree with the magnetic field of 304G within two standard deviations.

The  $\tilde{\omega}$  frequency can be used to disprove the estimations for the hyperfine parameters of Table 3.1, however if the measured values agree with the hyperfine estimation we cannot conclude that the estimations are correct.

For  $\tilde{\omega}$  the following frequencies were measured:  $\tilde{\omega}_{C1} = 2\pi \cdot 364.41 \pm 0.23\text{kHz}$  for carbon-1 and  $\tilde{\omega}_{C4} = 2\pi \cdot 371.52 \pm 0.39\text{kHz}$  for carbon-4. Based on the estimated hyperfine parameters we expect  $\tilde{\omega}_{C1} \approx 364.7\text{kHz}$  for carbon-1 and  $\tilde{\omega}_{C4} \approx 371.4\text{kHz}$  for carbon-4. Both these values are in good agreement with experiment, a good indication that our hyperfine estimation is accurate.

### Measuring $T_{2,C}^*$

In order to know how many operations we can perform on a qubit we must know how long the signal stays coherent under normal operation. In the case of controlling weakly carbons this is while decoupling the electron.

In order to determine carbon dephasing while decoupling the electron an uninitialized carbon-Ramsey was performed where the electron is decoupled during the free evolution time. Because the electron is constantly flipped the carbon will precess with an average frequency of  $\omega_{DD} = (\omega_L + \tilde{\omega})/2$ . By undersampling with a frequency slightly detuned from the precession frequency ( $\omega_{DD}$ ) a decaying cosine can be observed where the  $1/e$  time of the envelope is equal to  $T_{2,C}^*$ .

The decay for both carbons follows a Gaussian profile within uncertainty. The coherence times measured were  $T_{2,C1}^* = 9.85 \pm 0.39\text{ms}$  for carbon-1 and  $T_{2,C4}^* = 6.68 \pm 0.22\text{ms}$  for carbon-4.

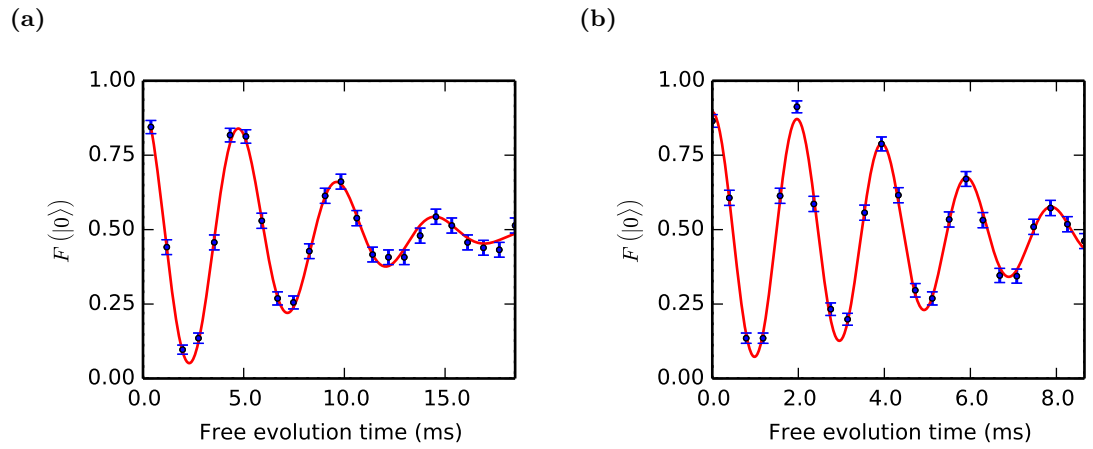


**Figure 3.8** – Carbon-Ramsey experiment to determine  $T_2^*$  for nuclei while decoupling the electron. The decays are fitted with a generalized normal distribution to determine  $T_2^*$  and the exponent  $n$ . Figure 3.8a, for carbon-1,  $T_{2,C1}^* = 9.85 \pm 0.39\text{ms}$  and  $n = 1.83 \pm 0.19$ . Figure 3.8b, for carbon-4,  $T_{2,C4}^* = 6.68 \pm 0.22\text{ms}$  and  $n = 2.31 \pm 0.31$ .

# 4

## Controlling Weakly-coupled Carbon Spins

Once the nuclear-spin environment of the NV-center has been characterized it is possible to control it. This chapter will demonstrate initialization, control and readout of weakly coupled carbon spins before explaining how an entangled state can be created using parity measurements. We will then demonstrate the created entanglement using quantum state tomography.

[Note intro needs to be rewritten once chapter is done]  
Now that we have identified several promising carbon spins we will go into controlling them.

In order to demonstrate entanglement we must be able to initialize the system, perform a parity measurement to create the entanglement and make a tomography to demonstrate it. This chapter will explain what operations need to be performed.

This chapter attempts to explain first how we can control a carbon by explaining how the two different rotation axes from the last chapter can be used to implement a conditional  $+X$  gate. A gate similar to a CNOT gate. Now that we understand how to implement a cnot gate we will use this to perform an experiment that we call a carbon ramsey on an uninitialized state. Afterwards we will use this to show that we can initialize and readout by showing an initialized carbon ramsey. (1bit tomo (ramsey with more T +Z-RO?). From this we will also determine  $T_{2C}^*$ .

The next section will consider two qubit control. It will start by explaining how we can perform a parity measurement. This measurement allows us to perform a two qubit tomography and create entanglement by projection. We will then show

### 4.1 Initialization and readout

The  $\pm x$ -gate can be used to initialize a carbon-spin. To initialize a carbon-spin in the  $|X\rangle$ -state the gate-circuit as depicted in Fig. 4.1a is implemented.

After the electronic-spin is brought in the  $|X\rangle$ -state the two-qubit system can be described by the tensor product of two density matrices:

$$\rho_X \otimes \rho_m = \rho_X \otimes \rho_X + \rho_X \otimes \rho_{-X} \quad (4.1)$$

By applying the  $\pm x$ -gate the electronic-spin picks up a phase depending on the nuclear spin-state:

$$\rho_Y \otimes \rho_X + \rho_{-Y} \otimes \rho_{-X} \quad (4.2)$$

The effect of the  $\pm x$ -gate can be made more easily understood by treating the carbon-spin as being either in the  $|X\rangle$  or  $|{-X}\rangle$ -state. Treating both as separate cases below.

$$|X\rangle|X\rangle \quad \vee \quad |X\rangle|{-X}\rangle \quad (4.3)$$

$$\frac{|0\rangle + |1\rangle}{\sqrt{2}}|X\rangle \quad \vee \quad \frac{|0\rangle + |1\rangle}{\sqrt{2}}|{-X}\rangle \quad (4.4)$$

$$\frac{e^{-i\pi/4}|0\rangle + e^{i\pi/4}|1\rangle}{\sqrt{2}}|X\rangle \quad \vee \quad \frac{e^{i\pi/4}|0\rangle + e^{-i\pi/4}|1\rangle}{\sqrt{2}}|{-X}\rangle \quad (4.5)$$

$$|Y\rangle|X\rangle \quad \vee \quad |{-Y}\rangle|{-X}\rangle \quad (4.6)$$

The final x-pulse is used to read out the electron. By conditionalizing the experiment on getting the outcome  $|0\rangle_e$  the carbon is initialized in the  $|X\rangle_C$ -state.

$$\rho_0 \otimes \rho_X + \rho_1 \otimes \rho_{-X} \quad (4.7)$$

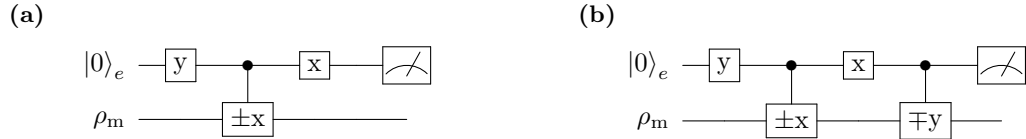


**Figure 4.1** – Figure 4.1a MBI-based initialization into  $\pm|X\rangle$ . Initializes the carbon into  $|X\rangle_C$  when  $|0\rangle_e$  is measured and into  $|-X\rangle_C$  when  $|1\rangle_e$  is measured for the electron. Figure 4.1b MBI-swap initialization into  $|0\rangle$ . Initializes the carbon into  $|0\rangle_C$  regardless of the electronic spin-state measured.

The sequence can be extended to a swap type initialization by implementing an additional  $\mp y$ -gate. The effect of the extra y-gate is that both the  $|X\rangle_C$  and the  $|-X\rangle_C$ -state are rotated to the  $|0\rangle_C$ -state, effectively swapping the mixed state from the carbon to the electron. By applying a readout the electron can be reinitialized.

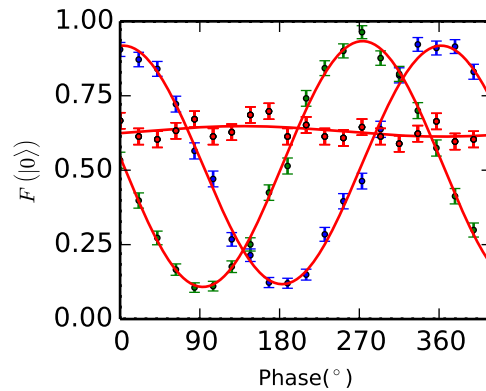


**Figure 4.2** – Demonstration of carbon control. Figure shows carbon-1

## 4.2 Parity measurement

Initialization by conditionalizing on parity measurement and Readout parities. Measurement projects into parity or no parity.

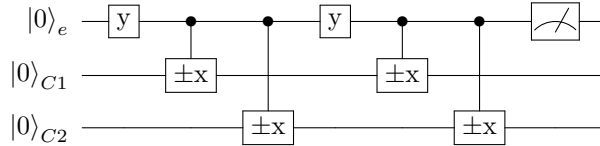


**Figure 4.3** – General parity RO

## 4.3 Demonstrating entanglement

### 4.3.1 Tomography

### 4.3.2 Result

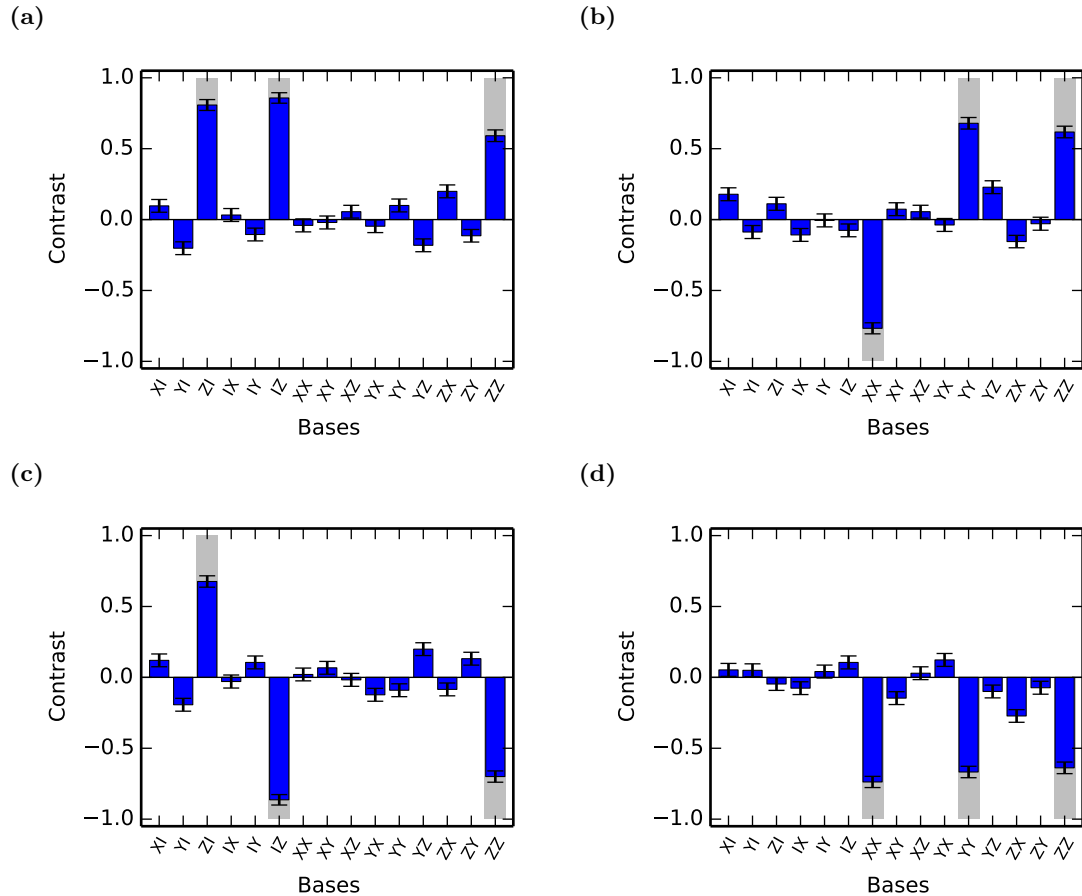


**Figure 4.4** – Preliminary data Fig. 4.4a Fidelity to guess = 0.814256440281 +/- 0.0168202298443  
Fig. 4.4b Fidelity to guess = 0.765954332553 +/- 0.0174228538115  
Fig. 4.4c Fidelity to guess = 0.809865339578 +/- 0.0168850158243  
Fig. 4.4d Fidelity to guess = 0.760831381733 +/- 0.0174356869379



# 5

## Outlook: towards Quantum Error Correction

This thesis has demonstrated the probabilistic creation of entangled states between weakly-coupled carbon spins. This chapter will provide an outlook on how the tools developed can be used to implement quantum error correction. It will also discuss the feasibility of using weakly-coupled carbon spins as a means to enlarge NV-spin registers in general

### 5.1 Direct outlook, deterministic operations/what needs to be done/can be done

### 5.2 Simulations, how many carbon can we control?



## Bibliography

- [1] H. Bernien. *Control, Measurement and Entanglement of Remote Quantum Spin Registers in Diamond*. PhD thesis, Delft University of Technology, 2014.
- [2] L. Childress and R. Hanson. Diamond nv centers for quantum computing and quantum networks. *MRS Bulletin*, 38(02):134–138, 2 2013. ISSN 0883-7694. URL [http://www.journals.cambridge.org/abstract\\_S0883769413000201](http://www.journals.cambridge.org/abstract_S0883769413000201).
- [3] G. de Lange. *Quantum Control and Coherence of Interacting Spins in Diamond*. PhD thesis, Delft University of Technology, 2012.
- [4] G. de Lange, Z.H. Wang, D. Rist, V.V. Dobrovitski, and R. Hanson. Universal dynamical decoupling of a single solid-state spin from a spin bath. *Science (New York, N.Y.)*, 330(6000):60–3, 10 2010. ISSN 1095-9203. URL <http://www.ncbi.nlm.nih.gov/pubmed/20829452>.
- [5] Marcus W. Doherty, Neil B. Manson, Paul Delaney, Fedor Jelezko, Jrg Wrachtrup, and Lloyd C.L. Hollenberg. The nitrogen-vacancy colour centre in diamond. *Physics Reports*, 528(1):1–45, 7 2013. ISSN 03701573. URL <http://linkinghub.elsevier.com/retrieve/pii/S0370157313000562>.
- [6] Richard P. Feynman. Simulating physics with computers. *International Journal of Theoretical Physics*, 21(6-7):467–488, 6 1982. ISSN 0020-7748. URL <http://link.springer.com/10.1007/BF02650179>.
- [7] Adam Gali. Identification of individual isotopes of nitrogen-vacancy center in diamond by combining the polarization studies of nuclear spins and first-principles calculations. *Physical Review B*, 80(24):241204, 12 2009. ISSN 1098-0121. URL <http://link.aps.org/doi/10.1103/PhysRevB.80.241204>.
- [8] Adam Gali, Maria Fyta, and Efthimios Kaxiras. Ab initio supercell calculations on nitrogen-vacancy center in diamond: Electronic structure and hyperfine tensors. *Physical Review B*, 77(15):155206, 4 2008. ISSN 1098-0121. URL <http://link.aps.org/doi/10.1103/PhysRevB.77.155206>.
- [9] Bas Jorrit Hensen. *Measurement-based Quantum Computation with the Nitrogen-Vacancy centre in Diamond*. PhD thesis, Delft University of Technology, 2011.
- [10] F. Jelezko, T. Gaebel, I. Popa, a. Gruber, and J. Wrachtrup. Observation of coherent oscillations in a single electron spin. *Physical Review Letters*, 92(7):076401, 2 2004. ISSN 0031-9007. URL <http://link.aps.org/doi/10.1103/PhysRevLett.92.076401>.
- [11] M.A. Nielsen and I.L. Chuang. *Quantum Computation and Quantum Information*. Cambridge University Press, 2010.
- [12] L. Robledo, L. Childress, H. Bernien, B. Hensen, P.F.A. Alkemade, and R. Hanson. High-fidelity projective read-out of a solid-state spin quantum register. *Nature*, 477(7366):574–8, 9 2011. ISSN 1476-4687. URL <http://www.ncbi.nlm.nih.gov/pubmed/21937989>.

- [13] P.W. Shor. Algorithms for quantum computation: discrete logarithms and factoring. In *Proceedings 35th Annual Symposium on Foundations of Computer Science*, pages 124–134. IEEE Comput. Soc. Press, 1994. ISBN 0-8186-6580-7. URL <http://ieeexplore.ieee.org/lpdocs/epic03/wrapper.htm?arnumber=365700>.
- [14] Benjamin Smeltzer, Lilian Childress, and Adam Gali. 13 c hyperfine interactions in the nitrogen-vacancy centre in diamond. *New Journal of Physics*, 13(2):025021, 2 2011. ISSN 1367-2630. URL <http://stacks.iop.org/1367-2630/13/i=2/a=025021?key=crossref.bdd6956722cde89a36ab3eee44a82724>.
- [15] T. H. Taminiau, J. J. T. Wagenaar, T. van der Sar, F. Jelezko, V. V. Dobrovitski, and R. Hanson. Detection and control of individual nuclear spins using a weakly coupled electron spin. *Physical Review Letters*, 109(13):137602, 9 2012. ISSN 0031-9007. URL <http://link.aps.org/doi/10.1103/PhysRevLett.109.137602>.
- [16] T. H. Taminiau, J.J.T. J. T. Wagenaar, T. van der Sar, F. Jelezko, V.V. V. Dobrovitski, and R. Hanson. Detection and control of individual nuclear spins using a weakly coupled electron spin. *Physical Review Letters*, 109(13):137602, 9 2012. ISSN 0031-9007. URL <http://link.aps.org/doi/10.1103/PhysRevLett.109.137602><http://arxiv.org/abs/1205.4128>.
- [17] T. H. TH Taminiau, J. Cramer, T. van der Sar, V. V. Dobrovitski, and R. Hanson. Universal control and error correction in multi-qubit spin registers in diamond. *Nature Nanotechnology*, 2(February):2–7, 9 2014. ISSN 1748-3387. URL <http://arxiv.org/abs/1309.5452><http://www.nature.com/doifinder/10.1038/nnano.2014.2>.
- [18] T. van der Sar, Z.H. Wang, M.S. Blok, H. Bernien, T.H. Taminiau, D.M. Toyli, D.A. Lidar, D.D. Awschalom, R. Hanson, and V.V. Dobrovitski. Decoherence-protected quantum gates for a hybrid solid-state spin register. *Nature*, 484(7392):82–6, 4 2012. ISSN 1476-4687. URL <http://www.ncbi.nlm.nih.gov/pubmed/22481361>.
- [19] L M Vandersypen, Matthias Steffen, Gregory Breyta, Costantino S Yannoni, Mark H Sherwood, and Isaac L Chuang. Experimental realization of shor’s quantum factoring algorithm using nuclear magnetic resonance. *Nature*, 414(6866):883–7, 2001. ISSN 0028-0836. URL <http://www.ncbi.nlm.nih.gov/pubmed/11780055>.

# A

## Fingerprintdata

The estimated hyperfine parameters of all 13 identified spins can be found in Table A.1. Due to the size of the fingerprint analysis it is not possible to include with this thesis. A pdf file containing the fingerprint analysis can be found here: <https://www.dropbox.com/s/gieji9e86bfvsf1/fingerprinting.pdf>.

Carbon	$A_{\parallel}$	$A_{\perp}$
1	$2\pi \cdot 30.0$ kHz	$2\pi \cdot 80.0$ kHz
2	$2\pi \cdot 27.0$ kHz	$2\pi \cdot 28.5$ kHz
3	$2\pi \cdot -51.0$ kHz	$2\pi \cdot 105.0$ kHz
4	$2\pi \cdot 45.1$ kHz	$2\pi \cdot 20.0$ kHz
5	$2\pi \cdot 17.0$ kHz	$2\pi \cdot 10.0$ kHz
6	$2\pi \cdot -15.0$ kHz	$2\pi \cdot 12.0$ kHz
7	$2\pi \cdot -23.0$ kHz	$2\pi \cdot 12.0$ kHz
8	$2\pi \cdot 10.0$ kHz	$2\pi \cdot 8.0$ kHz
9	$2\pi \cdot 8.0$ kHz	$2\pi \cdot 12.0$ kHz
10	$2\pi \cdot -9.3$ kHz	$2\pi \cdot 13.0$ kHz
11	$2\pi \cdot -10.0$ kHz	$2\pi \cdot 5.0$ kHz
12	$2\pi \cdot -30.0$ kHz	$2\pi \cdot 35.0$ kHz
13	$2\pi \cdot -32.0$ kHz	$2\pi \cdot 20.0$ kHz

**Table A.1** – Estimated hyperfine parameters for spins 1 to 13.



# B

## State Initialization

### B.1 Gates used

Gates are implemented according to Nielsen and Chuang [11].

$$R_j(\theta) = e^{-i\theta\sigma_i} \quad (\text{B.1})$$

Where  $\sigma_i$  are the pauli matrices:

$$\sigma_x = \frac{1}{2} \begin{bmatrix} 0 & 1 \\ 1 & 0 \end{bmatrix}, \quad \sigma_y = \frac{1}{2} \begin{bmatrix} 0 & -i \\ i & 0 \end{bmatrix}, \quad \sigma_z = \frac{1}{2} \begin{bmatrix} 1 & 0 \\ 0 & 1 \end{bmatrix} \quad (\text{B.2})$$

Such that:

$$\begin{aligned} R_x(\pi/2) &= \frac{1}{\sqrt{2}} \begin{bmatrix} 1 & -i \\ -i & 1 \end{bmatrix}, & R_x(-\pi/2) &= \frac{1}{\sqrt{2}} \begin{bmatrix} 1 & i \\ i & 1 \end{bmatrix}, & R_x(\pi) &= \begin{bmatrix} 0 & -i \\ -i & 0 \end{bmatrix} \\ R_y(\pi/2) &= \frac{1}{\sqrt{2}} \begin{bmatrix} 1 & -1 \\ 1 & 1 \end{bmatrix}, & R_y(-\pi/2) &= \frac{1}{\sqrt{2}} \begin{bmatrix} 1 & 1 \\ -1 & 1 \end{bmatrix}, & R_y(\pi) &= \begin{bmatrix} 0 & -1 \\ 1 & 0 \end{bmatrix} \\ R_z(\pi/2) &= \frac{1}{\sqrt{2}} \begin{bmatrix} (1-i) & 0 \\ 0 & (1+i) \end{bmatrix}, & R_z(-\pi/2) &= \frac{1}{\sqrt{2}} \begin{bmatrix} (1+i) & 0 \\ 0 & (1-i) \end{bmatrix}, & R_z(\pi) &= \begin{bmatrix} -i & 0 \\ 0 & i \end{bmatrix} \end{aligned}$$

Furthermore, we assume that a conditional gate applied by resonantly decoupling the electron always rotates the carbon-13 spin along  $\pm\hat{X}$ -axis. We call the conditional  $\pm x$ -gate **Ren**. Here  $\rho_i$  is the density matrix of a qubit in state  $i$ , multiple subscripts denote multiple qubits where the initial qubit is always the electron.

$$\mathbf{Ren} = \rho_0 \otimes R_x(\pi/2)_n + \rho_1 \otimes R_x(-\pi/2)_n \quad (\text{B.3})$$

With for a two-qubit system:

$$\mathbf{Ren} = \frac{1}{\sqrt{2}} \begin{bmatrix} 1 & -i & 0 & 0 \\ -i & 1 & 0 & 0 \\ 0 & 0 & 1 & i \\ 0 & 0 & i & 1 \end{bmatrix} \quad (\text{B.4})$$

An unconditional rotation is given by Eq. (B.5).

$$R_j(\theta)_e = R_j(\theta) \otimes \mathbf{I} \quad (\text{B.5})$$

### B.2 Initialization of the carbon-spin

Where in order to initialize into the  $|X\rangle_C$ -state we apply the circuit depicted in Fig. 4.1a. The electron starts in the  $|0\rangle$ -state and the carbon starts in a mixed state. We treat the mixed state of the carbon as a 50/50 mixture of  $|+X\rangle$  and  $|-X\rangle$ .

Density matrices describing initial state:

$$\rho_0 \otimes \rho_X + \rho_0 \otimes \rho_{-X} \quad (\text{B.6})$$

After applying initial y-pulse

$$\rho_X \otimes \rho_X + \rho_X \otimes \rho_{-X} \quad (\text{B.7})$$

Critical step: applying the conditional  $\pm x$ -gate.

$$\rho_Y \otimes \rho_X + \rho_{-Y} \otimes \rho_{-X} \quad (\text{B.8})$$

After applying the final x-pulse

$$\rho_0 \otimes \rho_X + \rho_1 \otimes \rho_{-X} \quad (\text{B.9})$$

Conventionalizing upon reading out  $|0\rangle$  for the electron projects the nucleus in the  $|X\rangle$ -state.

This sequence can be extended to unconditionally initialize the carbon in  $|0\rangle$ . By applying a  $\pm y$ -gate after the final x-pulse, we arrive at the following density matrix. NOTE: it would make more sense to do  $\mp y$

$$\rho_0 \otimes \rho_0 + \rho_1 \otimes \rho_0 \quad (\text{B.10})$$

# C

## Bell State Tomography

Derivation, what would a tomography of the Psi+ state look like?



D

## Entanglement witness





## Simulations and Calculations for Number of Addressable Carbons

### E.1 Scaling of number of resonances with magnetic field

Starting from Eq. (3.1)

$$\tau = \frac{(2k+1)\pi}{2\omega_L + A_{||}} \quad (\text{E.1})$$

In the limit where  $\omega_L \gg A$  the number of resonances  $K$  of a single carbon between  $\tau = 0$  and  $\tau = T_{DD,e}$  scales linear with the magnetic field:  $N_k \propto \omega_L$ .

At the same time the width of these resonances decreases quadratically with magnetic field (Eq. (3.2)).

$$\Delta = \frac{A_{\perp}}{2\omega_L^2} \quad (\text{E.2})$$

Combining these two we find that the number of resonances  $N$  that fit between two orders to increase linearly with magnetic field.

$$N_k - N_{k-1} = \frac{\tau_{k+1} - \tau_k}{\Delta} \quad (\text{E.3})$$

$$N_k - N_{k-1} = \frac{2\pi}{2\omega_L + A_{||}} \cdot \frac{2\omega_L^2}{A_{\perp}} \quad (\text{E.4})$$

$$N_k - N_{k-1} = \frac{2\pi\omega_L}{A_{\perp}} \quad (\text{E.5})$$

Meanwhile the time it takes to implement a  $\pi/2$ -gate is given by Eq. (E.6) where  $N_{\pi/2}$  is the number of pulses required for a  $\pi/2$ -pulse.

$$T_{\pi/2} = N_{\pi/2}\tau \quad (\text{E.6})$$

Using Eq. (3.4), and noting that  $\hat{n}_0$  and  $\hat{n}_1$  are anti-parallel at the resonance condition, we can find  $N$  to be:

$$\frac{\pi}{4} = \frac{N_{\pi/2}\phi}{2} \quad (\text{E.7})$$

$$N_{\pi/2} = \frac{\pi}{2\phi} \quad (\text{E.8})$$

Where  $\phi$  is given by Eq. (3.6).

$$\phi = \cos^{-1} \left( \cos(\tilde{\omega}\tau) \cos(\omega_L\tau) - \left( \frac{A_{||} + \omega_L}{\tilde{\omega}} \right) \sin(\tilde{\omega}\tau) \sin(\omega_L\tau) \right) \quad (\text{E.9})$$

In the limit where  $\omega_L \gg A$ ,  $\omega_L \approx \tilde{\omega}$  simplifying Eq. (E.9) to:

$$\phi = \cos^{-1} (\cos^2(\omega_L\tau) - \sin^2(\omega_L\tau)) \quad (\text{E.10})$$

$$\phi = \cos^{-1} (2 \cos(\omega_L\tau)) \quad (\text{E.11})$$



# F

## Constants and Experimental values

Gyromagnetic Ratios

$\gamma_e$	$2\pi \cdot 2.8025$	MHz/G
$\gamma_N$	$2\pi \cdot 0.3077$	kHz/G
$\gamma_C$	$2\pi \cdot 1.0705$	kHz/G

Interaction Strengths

$\Delta$	$2\pi \cdot 2.878$	GHz
$Q$	$2\pi \cdot 4.946$	MHz
$A_N$	$2\pi \cdot 2.186$	MHz

Optics

637 nm	471 THz
--------	---------



## **Acknowledgements**